frontiers | Frontiers in Chemistry

TYPE Original Research
PUBLISHED 29 September 2022
DOI 10.3389/fchem.2022.963203

OPEN ACCESS

EDITED BY
Wei Zeng,
Northwest Normal University, China

REVIEWED BY
Shaowei Zhang,
Hunan University of Science and Technology, China
Cai-Ming Liu,
Institute of Chemistry (CAS), China

*CORRESPONDENCE
Jin Wang,
wangjin110@ntu.edu.cn
Yuanyuan Peng,
pengyy@sustech.edu.cn
Yanfeng Tang,
tangyf@ntu.edu.cn

†These authors have contributed equally to this work

SPECIALTY SECTION
This article was submitted to Solid State Chemistry, a section of the journal Frontiers in Chemistry

RECEIVED 07 June 2022
ACCEPTED 09 September 2022
PUBLISHED 29 September 2022

CITATION
Wang M, Sun C, Gao Y, Xue H, Huang L, Xie Y, Wang J, Peng Y and Tang Y (2022), Three Gd-based magnetic refrigerant materials with high magnetic entropy: From di-nuclearity to hexa-nuclearity to octa-nuclearity.
Front. Chem. 10:963203.
doi: 10.3389/fchem.2022.963203

Three Gd-based magnetic refrigerant materials with high magnetic entropy: From di-nuclearity to hexa-nuclearity to octa-nuclearity

Minmin Wang[1†], Chengyuan Sun[1†], Yujia Gao[1], Hong Xue[1], Ling Huang[1], Yutian Xie[1], Jin Wang[1*], Yuanyuan Peng[2*] and Yanfeng Tang[1*]

[1]School of Chemistry and Chemical Engineering, Nantong University, Nantong, China, [2]Department of Chemistry, Southern University of Science and Technology, Shenzhen, China

Magnetocaloric effect (MCE) is one of the most promising features of molecular-based magnetic materials. We reported three Gd-based magnetic refrigerant materials, namely, $Gd_2(L)(NO_3)(H_2O)\cdot CH_3CN\cdot H_2O$ (**1**, H_2L = (*Z*)-*N*-[(1*E*)-(2-hydroxy-3-methphenyl)methylidene]pyrazine-2-carbohydrazonic acid), $\{Gd_6(L)_6(CO_3)_2(CH_3OH)_2(H_2O)_3Cl\}Cl\cdot 4CH_3CN$ (**2**), and $Gd_8(L)_8(CO_3)_4(H_2O)_8\cdot 2H_2O$ (**3**). Complex **1** contains two Gd^{III} ions linked by two $\eta^2{:}\eta^1{:}\eta^1{:}\eta^1{:}\mu_2$-$L^{2-}$ ligands, which are seven-coordinated in a capped trigonal prism, and complex **2** possesses six Gd^{III} ions, contributing to a triangular prism configuration. For complex **3**, eight Gd^{III} ions form a distorted cube arrangement. Moreover, the large values of magnetic entropy in the three complexes prove to be excellent candidates as cryogenic magnetic coolants.

KEYWORDS

magnetocaloric effect, polynuclear, lanthanide, Schiff-based ligand, magnetic entropy

Introduction

Ln-based complexes play a critical role in molecular-based materials not only due to the charming geometrical structures but also because of the extensive applications such as luminescence, catalysis, especially for magnetic materials including magnetocaloric effect (MCE) (Wu D et al., 2020; Shang et al., 2021; Wei et al., 2021), and single-molecule magnets (SMMs) (Liu et al., 2014; Liu et al., 2016; Zhang and Cheng, 2016; Reis, 2020). As a member of the Ln elements, the Gd ion is a perfect candidate in the synthesis of molecular-based magnetic refrigeration materials because of the large magnetothermal effects (Evangelisti et al., 2011; Chen et al., 2013; Chen et al., 2014; Wang et al., 2020a; Li et al., 2021; Lin et al., 2021; Wu T et al., 2021; Zhou et al., 2021). Some of the reported magnetic materials even possess a large cryogenic MCE, which is comparable to that of the commercial coolant $\{Gd_3Ga_5O_{12}\}$ (Pecharsky and Gschneidner, 1997; Zhang S. et al., 2015; Zhang S.,-W. et al., 2015).

It is worth mentioning that in the pure 4f system, improving magnetic density is the ideal method to gain MCE performance (Zhang et al., 2016; Reis, 2020). Therefore, organic ligands play an important role in the building units of the complexes. In previous studies, various organic ligands (e. g. Schiff-based ligands (Aronica et al., 2006; Boulon et al., 2013; Mannini et al., 2014; Burgess et al., 2015; Nava et al., 2015; Wang et al., 2015; Lakma et al., 2019; Li et al., 2019; Wang et al., 2020b; Wang J. et al., 2021; Wang M. et al., 2021), carboxylates (Milios et al., 2007; Dermitzaki et al., 2015; Yin et al., 2015; Botezat et al., 2017; Feltham et al., 2017; Li et al., 2019; Zheng et al., 2020; Han et al., 2021; Zhou et al., 2021), diketones (Zhu et al., 2014; Yao et al., 2018; Wang et al., 2019a; Wang et al., 2019b; Shi et al., 2021), and diamines (Neves et al., 1992; Zhang et al., 2013; Cornia et al., 2014; Oyarzabal et al., 2014; Feltham et al., 2015; Luan et al., 2015; Lu et al., 2019) etc.) have been successfully utilized in the synthesis of MCE materials. Among them, Schiff-based ligands comprise rich O and N sites, which are widely used in the synthesis of many Ln complexes because of the simple synthesis and structural diversity.

In this work, three Gd-based magnetic refrigerant materials based on Schiff-based ligands (*Z*)-*N*-[(1*E*)-(2-hydroxy-3-methphenyl) methylidene]pyrazine-2-carbohydrazonic acid (H_2L) were synthesized, namely, $Gd_2(L)(NO_3)(H_2O)\cdot CH_3CN\cdot H_2O$ (**1**), $\{Gd_6(L)_6(CO_3)_2(CH_3OH)_2(H_2O)_3Cl\}Cl\cdot 4CH_3CN$ (**2**), and $Gd_8(L)_8(CO_3)_4(H_2O)_8\cdot 2H_2O$ (**3**). Magnetic studies indicate that all complexes exhibit antiferromagnetic interactions between the spin centers and display large magnetic entropies.

Materials and methods

Materials

All reactions and manipulations were performed in the ambient atmosphere. The Schiff-based H_2L ligand was prepared by condensation with *o*-vanillin and hydrazine-2-carbohydrazide in methanol according to the literature (Chandrasekhar et al., 2013; Chen et al., 2016). Metal salts and other reagents were commercially available and used without further purification.

Synthesis

Synthesis of $Gd_2(L)_2(NO_3)_2(H_2O)_2\cdot CH_3CN\cdot H_2O$ (**1**): a mixture of H_2L (0.1 mmol, 27.2 mg) and $Gd(NO_3)_3\cdot 6H_2O$ (0.1 mmol, 45.7 mg) was dissolved in CH_3CN (5 ml) and CH_3OH (2.5 ml). After stirring for 5 min, pyridine (0.04 ml) was added and stirred for another 10 min. The solution was filtered and left to slowly evaporate. Well-shaped orange crystals were obtained after 1 week. Yield: 20 mg, 36% based on Gd. Elemental analysis (EA) calc. (%) for $Gd_2C_{30}H_{30}N_{12}O_{16}$, C: 31.91, H: 2.68, N: 14.89; found (%), C: 32.03, H: 2.61, N: 14.93.

$\{Gd_6(L)_6(CO_3)_2(CH_3OH)_2(H_2O)_3Cl\}Cl\cdot 4CH_3CN$ (**2**): a mixture of H_2L (0.2 mmol, 54.4 mg) and $GdCl_3.6H_2O$ (0.2 mmol, 74.3 mg) was dissolved in CH_3CN (10 ml) and CH_3OH (5 ml). After stirring for 5 min, $NaHCO_3$ (0.2 mmol, 33.6 mg) was added and stirred for another 3 h. Well-shaped orange crystals were obtained after 1 week. Yield: 32 mg, 32% based on Gd. Elemental analysis (EA) calc. (%) for $Gd_6C_{90}H_{92}N_{28}O_{29}Cl_2$, C: 35.51, H: 3.05, N: 12.88; found (%), C: 35.72, H: 2.99, N: 12.92.

$Gd_8(L)_8(CO_3)_4(H_2O)_8\cdot 2H_2O$ (**3**): a mixture of H_2L (0.2 mmol, 13.6 mg) and $GdCl_3.6H_2O$ (0.2 mmol, 18.6 mg) was dissolved in CH_3CN (5 ml) and CH_3OH (2.5 ml). After stirring for 5 min, $NaCO_3$ (0.2 mmol, 10.6 mg) was added and stirred for another 2 h. Well-shaped orange crystals were obtained after 1 week. Yield: 28 mg, 29% based on Gd. Elemental analysis (EA) calc. (%) for $Gd_8C_{108}H_{100}N_{32}O_{46}$, C: 33.78, H: 2.62, N: 11.67; found (%), C: 33.83, H: 2.51, N: 11.84.

Physical measurements

The C, H, and N elemental analyses were performed using an Elementar Vario-EL CHNS elemental analyzer. The Fourier transform-infrared (FT-IR) spectra were carried out from KBr pellets in the range 4,000–400 cm^{-1} using an EQUINOX 55 spectrometer. Powder X-ray diffraction (PXRD) patterns were performed using the Bruker D8 Advance diffractometer (Cu–*K*α, λ = 1.54056 Å). Magnetic susceptibility measurements were measured with a Quantum Design MPMS-XL7 SQUID. Polycrystalline samples were embedded in vaseline to prevent torquing. Data were corrected for the diamagnetic contribution calculated from Pascal constants.

Crystallographic study

Suitable single crystals for **1–3** were selected for single-crystal X-ray diffraction analysis. Data were collected using a Rigaku Oxford diffractometer with a Mo–Kα radiation (λ = 0.71073 Å) at 120 K. The structures were solved by direct methods and refined by least-squares on F^2 utilizing the SHELXTL program suite and Olex2 (Dolomanov et al., 2009; Sheldrick, 2015a,b). The hydrogen atoms were set in calculated positions and refined as riding atoms with common fixed isotropic thermal parameters. EA was used to detect the content of C, H, and N atoms. Detailed information about the crystal data and structure refinements is summarized in Table 1. Selected bond lengths and angles of complexes **1–3** are listed in Supplementary Table S1–S3.

TABLE 1 Crystallographic data and structural refinement parameters for complexes 1–3.

Complex	1	2	3
Formula	$Gd_2(L)_2(NO_3)_2(H_2O)_2{\cdot}CH_3CN{\cdot}H_2O$	$\{Gd_6(L)_6(CO_3)_2(CH_3OH)_2(H_2O)_3Cl\}Cl{\cdot}4CH_3CN$	$Gd_8(L)_8(CO_3)_4(H_2O)_8{\cdot}2H_2O$
M_r [g·mol^{-1}]	1127.17	3044.31	3840.19
T [K]	120 (2)	120 (2)	120 (2)
Crystal system	Triclinic	Triclinic	Triclinic
Space group	P-1	P-1	P-1
a [Å]	8.8137 (8)	13.5408 (9)	17.84766 (16)
b [Å]	9.4123 (9)	18.8679 (15)	18.2321 (2)
c [Å]	13.3026 (12)	23.2844 (16)	28.0616 (3)
α [°]	95.912 (3)	90.424 (3)	73.0978 (10)
β [°]	109.101 (3)	92.888 (2)	77.7530 (8)
γ [°]	107.900 (3)	106.296 (2)	61.2890 (11)
V [Å^3]	966.55 (16)	5701.2 (7)	7634.03 (16)
Z	1	2	2
ρ_{calcd} [g·cm^{-3}]	1.936	1.773	1.671
μ [mm^{-1}]	3.487	3.569	3.506
F (000)	550.7	2956.0	3704.0
Refl.collected/unique	8376/3895	70871/25093	124216/39110
GOF on F^2	1.0385	1.030	1.033
R_1/wR_2 [$I > 2\sigma(I)$, squeeze] [a]	0.0379/0.0963	0.0393/0.0943	0.0378/0.0887
R_1/wR_2 (all data, squeeze)	0.0424/0.1001	0.0454/0.0995	0.0512/0.0946
CCDC No.	2174539	2174540	2174541

[a]$R_1 = \sum||F_o| - |F_c||/\sum|F_o|$. $wR_2 = [\sum w (F_o^2-F_c^2)^2/\sum w (F_o^2)^2]^{1/2}$.

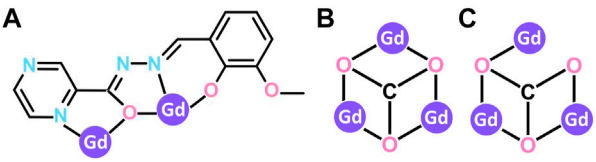

SCHEME 1
Coordination modes of L^{2-} ligand **(A)** and CO_3^{2-} **(B,C)**.

Results and discussion

Description of the structures of **1–3**

Complexes **1–3** are synthesized by the evolution method with H_2L and gadolinium salt in the solution of CH_3CN/CH_3OH (V_1: V_2 = 2:1) under the existence of alkali. The alkali is added to be conducive to protonate the ligand H_2L, which is beneficial to incorporate Gd^{III} ions. The H_2L ligand in all complexes is completely dehydrogenated adopting the μ_2:η^2:η^1:η^1:η^1-mode (Scheme 1A), which is similar to the reported literature (Chandrasekhar et al., 2013; Chen et al., 2016; Zhang et al., 2017; Zhang et al., 2016; Jiang et al., 2016).

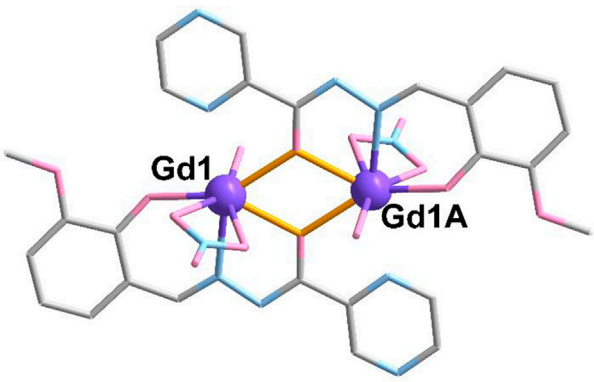

FIGURE 1
Crystal structure of complex **1**. The hydrogen atoms are omitted for clarity. Color codes: Gd, purple; O, pink; N, blue; and C, grey. Symmetric code: A, 1-x, 1-year, and 1-z.

Complex **1** is crystalized in the triclinic P-1 space group. As shown in Figure 1, the crystallography independent unit of **1** contains half of the molecule, including one Gd^{III} ion, one L_2^- ligand, one NO_3^- anion, and half of CH_3CN and H_2O molecules. The metallic Gd^{III} ions (Gd1 and Gd1A) are surrounded by two L_2^- ligands using the aforementioned

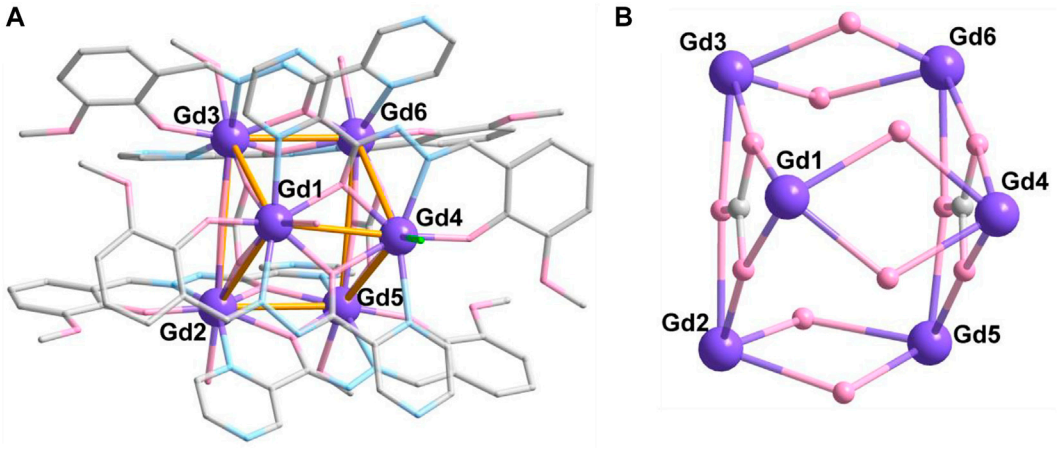

FIGURE 2
Crystal structure **(A)** and metallic core **(B)** of complex **2**. The hydrogen atoms are omitted for clarity. Color codes: Gd, purple; O, pink; N, blue; and C, gray.

mode, two NO_3^- anions and two H_2O molecules located above and below the plane, respectively. The average bond lengths of Gd-O and Gd-N are 2.379 (5) Å and 2.460 (5) Å (Supplementary Table S1), respectively, which are in accordance with those of the reported Gd-based complexes (Chen et al., 1995; Zhao et al., 2017; Mayans and Escuer, 2021; Ren et al., 2021). In complex **1**, the Gd ion is seven-coordinated to form a capped trigonal prism, which is confirmed by CShM calculations (Alvarez et al., 2005; Casanova et al., 2005) (Supplementary Figure S1, Supplementary Table S4).

Complex **2** crystalizes in the same space group as complex **1**, and the asymmetric unit comprises the whole molecule with six crystallographically independent Gd^{III} ions (Figure 2A). The six Gd ions are held together to form a $\{Gd_6\}$ triangular prism metallic skeleton (Figure 2B). Therein, three Gd ions in the plane (Gd1, Gd2, and Gd3 or Gd4, Gd5, and Gd6) contribute a triangular configuration, which are bridged by one CO_3^{2-} anion in μ_3-η^2:η^2:η^2-mode (Scheme 1B). The two triangular metallic skeletons are then linked together by six μ_2-O bridges from ligands.

All Gd ions are eight coordinated, showing two kinds of coordination geometry confirmed by CShM calculations (Alvarez et al., 2005; Casanova et al., 2005) (Supplementary Table S5). The Gd1, Gd2, Gd3, Gd5, and Gd6 ions are in $\{O_6N_2\}$ environment with six O atoms and two N atoms from two chelated L^{2-} ligands, one CO_3^{2-} anion and one CH_3OH/H_2O molecule, which display a biaugmented trigonal prism configuration (Supplementary Figure S2). The average Gd-O and Gd-N distances are 2.352 (4) Å and 2.475 (4) Å, respectively (Supplementary Table S2), which are consistent with those reported Gd-based complexes (Chen et al., 1995; Zhao et al., 2017; Mayans and Escuer, 2021; Ren et al., 2021). However, Gd4 has triangular dodecahedron coordination geometry and is located in an $\{O_5N_2Cl\}$ environment with five O and two N atoms from two chelated L^{2-} ligands and one Cl^- anion. The bond length of Gd4-Cl1 is 2.746 (1) Å, which is longer than that of Gd-O and Gd-N.

For complex **3**, the synthetic method is the same as complex **2**; except $NaHCO_3$ was used in place of Na_2CO_3. Surprisingly, complex **3** possesses an octa-nuclearity structure, which crystalizes in the triclinic *P*-1 space group. The asymmetric unit consists of a completed molecule, and there are eight crystallographically independent Gd atoms in the molecular structure (Figure 3A). As shown in Figure 3B, the eight Gd^{III} ions contribute to a cubic trapezoid metallic core. Gd1, Gd4, Gd5, and Gd8 ions lie in the four vertices of the plane below the cubic trapezoid, while Gd2, Gd3, Gd6, and Gd7 ions situate in the upper plane. The metallic core is held together by four CO_3^{2-} anions in μ_3-η^2:η^2:η^1-mode (Scheme 1C). The periphery of the metal core is ligated by eight L^{2-} ligands, eight H_2O molecules, and two lattice H_2O molecules.

There are two coordination numbers of Gd^{III} ions in complex **3** (Supplementary Figure S3). Gd1, Gd3, Gd5, and Gd7 are eight-coordinated ions in $\{O_6N_2\}$ donor set from two L^{2-} ligands, two CO_3^{2-} anions, and one H_2O molecule, while Gd2, Gd4, Gd6, and Gd8 ions are nine-coordinated in the $\{O_7N_2\}$ donor set. The difference between the two kinds of Gd ions is the diverse coordination modes of the CO_3^{2-} anion. There is only one coordination bond of O atom in CO_3^{2-} anion, which is adopted in Gd1, Gd3, Gd5, and Gd7 ions. For Gd2, Gd4, Gd6, and Gd8 ions, the bonding mode of the CO_3^{2-} anion is adopted in the bidentate mode. The eight metal ions exhibit three coordination geometries: biaugmented trigonal prism (Gd1), triangular dodecahedron (Gd3, Gd5, and Gd7), and muffin

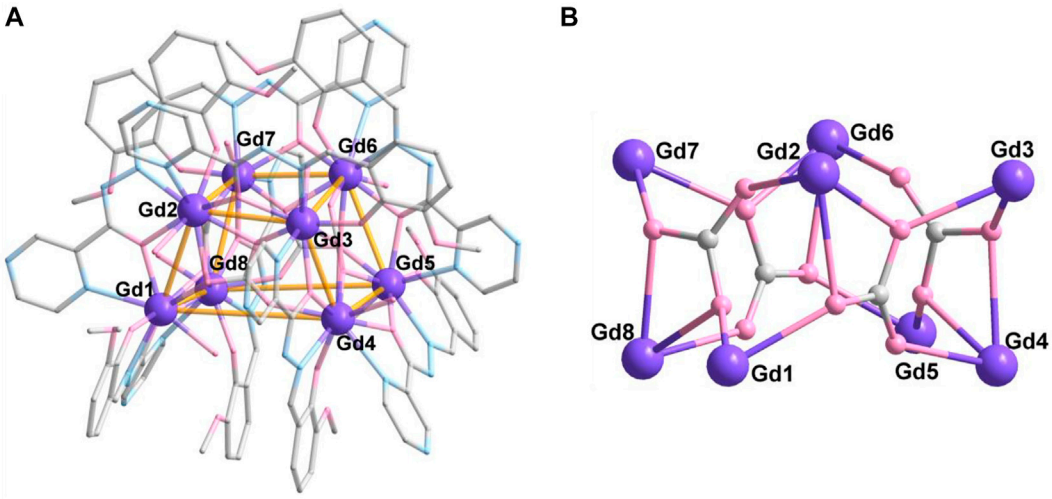

FIGURE 3
Crystal structure **(A)** and metallic core **(B)** of **3**. The hydrogen atoms are omitted for clarity. Color codes: Gd, purple; O, pink; N, blue; and C, gray.

(Gd2, Gd4, Gd6, and Gd8) (Supplementary Tables S5,6). The average Gd-O distance is 2.361 (4) Å, which is shorter than that of Gd-N (2.564 (4) Å) lengths. The O/N-Gd-O/N angles are in the range of 60.99°–154.86°, which are in the normal range (Chen et al., 1995; Zhao et al., 2017; Mayans and Escuer, 2021; Ren et al., 2021).

It is worth mentioning that the use of different alkalis can affect the number of formed metal nuclearity. For the organic weak alkali triethylamine, which is used in complex **1**, it only facilitates protonation of the ligand H_2L but is not involved in the final formation of complex **1**. However, for complexes **2** and **3**, the inorganic alkalis not only deprotonate the ligand but also participate in the construction of the molecules. Compared to $NaHCO_3$ in complex **2**, the alkalinity of Na_2CO_3 is relatively strong. Moreover, mainly due to the degree of hydrolysis of carbonates being higher, there are more carbonate triangle skeletons in complex **3**, making it easier to coordinate with Gd ions, thus forming an octa-nuclearity complex.

IR spectra and PXRD studies

The FT-IR spectra of complexes **1–3** were acquired (ν = 4,000–500 cm^{-1}), which are shown in Supplementary Figure S4. Powder X-ray diffraction (PXRD) measurements for complexes **1–3** were performed for the crystalline crystals (Supplementary Figure S5), and the experimental patterns are in good agreement with the simulated ones from the crystallographic data. The minor inconsistencies in the intensity and shape of the peaks indicate the phase purity of complexes **1–3**.

Magnetic studies

The direct current magnetic susceptibilities of complexes **1–3** were studied for polycrystalline samples in the temperature range of 2–300 K at an external magnetic field of 1000 Oe (Figure 4A). At room temperature, the $\chi_M T$ values of complexes **1–3** are 15.77, 47.16, and 62.81 $cm^3\,K\,mol^{-1}$, respectively, which is in good agreement with the expected spin-only values (Gd^{III} ion: 7.875 $cm^3\,K\,mol^{-1}$, g = 2). Upon cooling, the $\chi_M T$ values in all cases stay essentially unchanged until approximately 25 K and then followed by an obvious decrease to the minimum values of 13.29, 38.46, and 58.30 $cm^3\,K\,mol^{-1}$, indicating antiferromagnetic interactions (Kahn et al., 2000). Fitting the curve of χ_M^{-1} vs. T with the Curie–Weiss Law (Figure 4B) gives the resulting C and θ values, which are listed in Supplementary Table S7. The negative θ values imply the presence of weak antiferromagnetic interaction within complexes **1–3**.

The field dependence of the magnetization plots for complexes **1–3** was performed in the field range of 1–7 T at 2–8 K (Supplementary Figure S6). Magnetizations in all complexes are increased gradually at the entire field region, reaching saturation values of 13.81, 41.75, and 55.83 $N\mu_B$ at 7 T and 2 K, respectively, close to the theoretical value (**1**: 14 $N\mu_B$; **2**: 42 $N\mu_B$; **3**: 56 $N\mu_B$). The reduced magnetization plots (M vs. HT^{-1}) in all complexes are superposable due to the isotropic system (Supplementary Figure S7).

Due to the complicated systems in complexes **2** and **3**, only complex **1** is attempted to analyze the magnetic interactions by using a simplified spin Hamiltonian with the PHI program (Eq. 1):

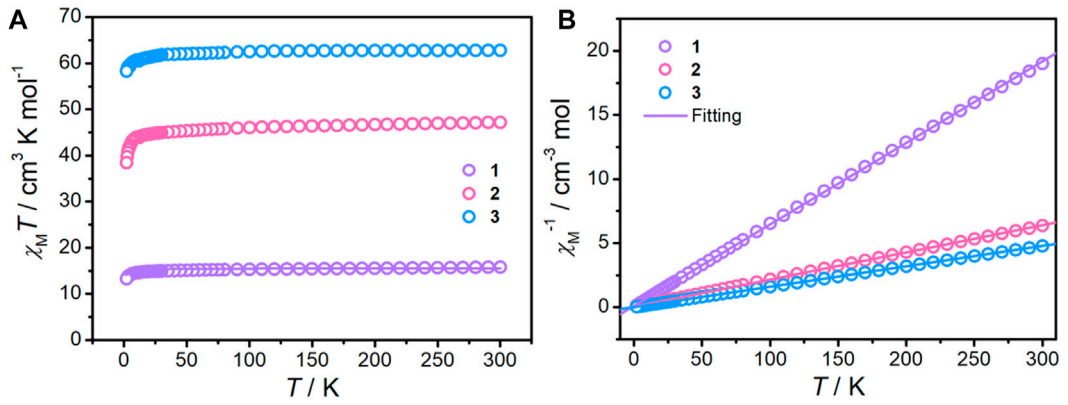

FIGURE 4
$\chi_M T$ products measured under a 1000 Oe DC applied field **(A)** and the plots of $1/\chi_M$ vs. T **(B)** for complexes **1**–**3**. The solid lines represent the best fitting.

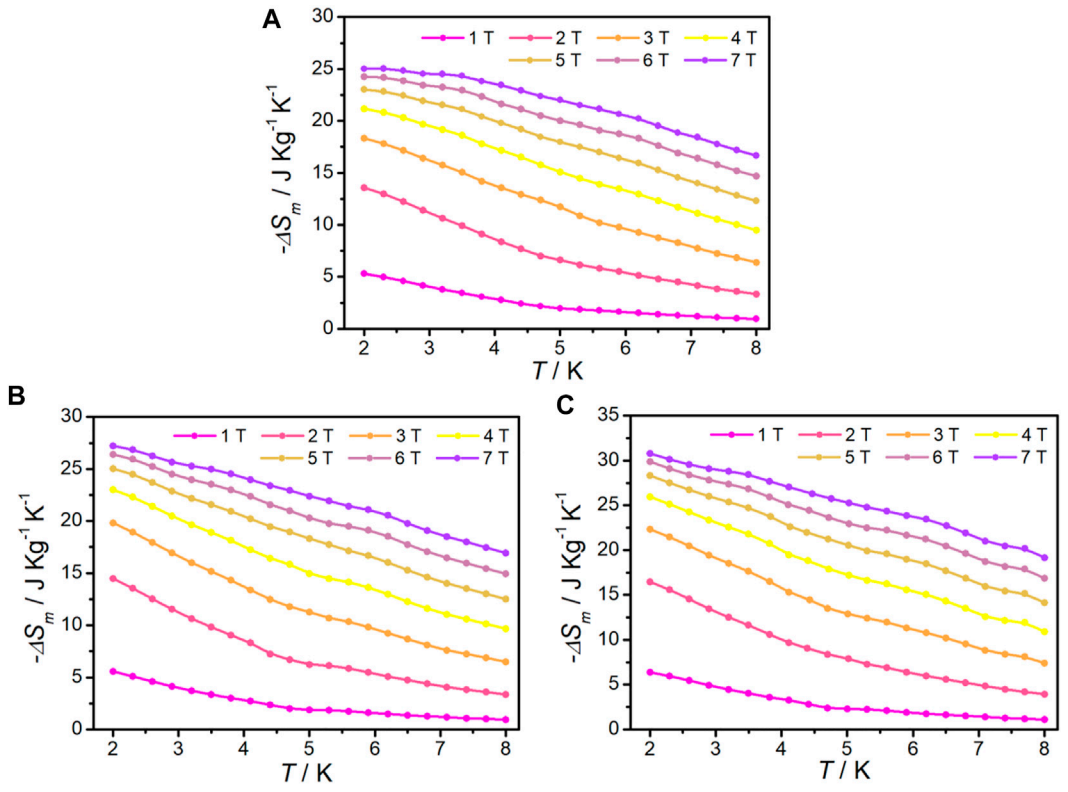

FIGURE 5
-ΔS_m at various fields and temperatures, calculated from the magnetization data for **1(A)**, **2(B)**, and **3(C)**.

$$\hat{H}_{\mathrm{Gd-Gd}} = -2J_{\mathrm{Gd-Gd}}\hat{S}_{\mathrm{Gd1}}\hat{S}_{\mathrm{Gd2}}. \quad (1)$$

The best-fit parameters are J = -0.022 (2) cm^{-1} and g = 1.98 (Figure 4A; Supplementary Figure S8). The negative J value confirms the antiferromagnetic interactions between the Gd^{III} ions, which is in accordance with the trend of the $\chi_M T$ product with cooling and the result of the Curie–Weiss Law.

The isothermal magnetization for complexes **1–3** was measured from 2 to 8 K in an applied DC field up to 7 T to calculate the magnetic entropy (-ΔS_m) according to the Maxwell equation (Pecharsky and Gschneidner, 1999)

TABLE 2 Summary of -ΔS_m in different ΔH at a given temperature for reported di-nuclearity, hexa-nuclearity, octa-nuclearity, and other multinuclear Gd-based complexes.

Complex	-ΔS_m [J kg^{-1} K^{-1}]	ΔH [T], T [K]	Ref
$\{Gd_2(OAc)_6(H_2O)_4\}\cdot 4H_2O$	40.6	7, 1.8	Evangelisti et al. (2011)
$Gd_2(OAc)_2(Ph_2acac)_4$ $(MeOH)_2$	23.7	7, 2.4	Guo et al. (2012)
Gd_2 $(hfac)_4$ $(fpmoq)_2$	17.1	8, 3.0	Wang et al. (2015)
Gd_2 $(hfac)_4$ $(btoq)_2$	16.9	8, 2.0	Shen et al. (2015)
Gd_2 (L_1) $(dbm)_5$	17.69	8, 2.0	Wang et al. (2021a)
Gd_2 $(iba)_6$ $(bipy)_2$	29.3	7, 2.0	Zhou et al. (2021)
Gd_2 $(nic)_6(H_2O)_4$	27.4	7, 2.0	Zhou et al. (2021)
$Gd_2(L)_2(CH_3OH)_2$	24.75	7, 2.0	Shi et al. (2020)
$\{Gd_2(L)_2$ $(dbm)_2(H_2O)_2\}\cdot nCH_3OH$	23.2	7, 2.0	Shi et al. (2021)
Gd_2 $(dnba)_6$ $(phen)_2$	16.8	7, 2.0	Zheng et al. (2020)
$Gd_2(Hnsa)_2$ $(nsa)_2$ $(phen)_2(H_2O)_2$	22.2	7, 2.0	Zheng et al. (2020)
1	25.05	7, 2.0	This work
$\{Gd_6$ $(bobdz)_2(HCO_2)_4$ $(\mu_3\text{-}OH)_4$ $(DMF)_6(H_2O)_2\}Cl_2\cdot 4H_2O$	33.5	7,3.0	Adhikary et al. (2014)
$Gd_6(L)_2$ $(acac)_6(OH)_4(NO_3)_2(CH_3OH)_2$	35.3	7, 2.0	Wang et al. (2020b)
$\{H_2$ $[Gd_6(OH)_8(H_2O)_6$ $(p\text{-}BDC\text{-}F_4)_6]\}\cdot 3$ $(2,2'\text{-}bpy)\cdot 6H_2O$	28.27	7, 2.0	Wei et al. (2019)
$\{H_2$ $[Gd_6(OH)_8(H_2O)_6$ $(m\text{-}BDC\text{-}F_4)_6]\}\cdot 3$ $(4,4'\text{-}bpy)\cdot 6H_2O$	29.20	7, 2.0	Wei et al. (2019)
2	27.21	7, 2.0	This work
$\{Gd_8(IN)_{14}$ $(\mu_3\text{-}OH)_8$ $(\mu_2\text{-}OH)_2(H_2O)_8\}\cdot 11H_2O$	31.77	7, 2.0	Shi et al. (2020)
$\{Gd_8$ $(\mu_3\text{-}O)_4(L)_8(CH_3COO)_4(CO_3)_2\}\cdot 15H_2O$	32.49	7, 2.0	Li et al. (2019)
3	30.79	7, 2.0	This work
$\{Gd_3$ $(dbm)_5(HL)_2\}\cdot 4CH_3OH\cdot 3CH_2Cl_2$	20.60	7, 2.0	Wang et al. (2020c)
$\{Gd_3(HL)$ (H_2L) $(NO_3)_4\}\cdot C_2H_5OH$	30.22	7, 2.0	Wang et al. (2019c)
$\{Gd_4(H_3L)_2(OAc)_3(F_6acac)_3\}\cdot 4MeOH\cdot 2.5H_2O$	21.88	5, 2.0	Liu and Hao, (2022)
$\{Gd_4$ $(acac)_4$ $(\mu_3\text{-}OH)_2L_6\}\cdot 2CH_3CN$	14.57	7, 3.0	Hou et al. (2020)
$\{Gd_4(HL)_4(CH_3O)_4\}\cdot 3CH_3OH$	30.42	7, 2.0	Li et al. (2020)
$\{Gd_4(L)_4$ $(m_2\text{-}CH_3O)_4\}\cdot CH_3OH$	28.50	7, 2.0	Xu et al. (2021)
$\{Gd_4$ $(acac)_4(L)_6$ $(\mu_3\text{-}OH)_2\}\cdot CH_3CN$	24.46	7, 2.0	Wang et al. (2020d)

(Eq. 2). It can be seen that the curves of -ΔS_m of complexes **1–3** gradually increase with decreasing temperature and increasing of magnetic field without saturation, the maximum -ΔS_m values are 25.05 J kg^{-1} K^{-1}, 27.21 J kg^{-1} K^{-1}, and 30.79 J kg^{-1} K^{-1} at 2 K, ΔH = 7 T, respectively (Figure 5). These values are smaller than the theoretical values of 34.57 J kg^{-1} K^{-1} for **1**, 34.07 J kg^{-1} K^{-1} for **2**, and 36.01 J kg^{-1} K^{-1} for **3**, which are calculated using Eq 3, (n = 2, 6, and 8 for **1**, **2**, and **3**, respectively; S = 7/2 and the R value is 8.314 J mol^{-1} K^{-1}), owing to the existence of antiferromagnetic coupling. The maximum -ΔS_m of **1** in di-nuclearity complex is among the highest observed to date for 4f clusters appeared at low temperature (Table 2). Although complexes **2** and **3** do not possess the highest -ΔS_m values, they are still comparable in the same nuclear complexes.

$$\Delta S_m(T) = \int_0^H [\partial M(T,H)/\partial T]_H dH, \quad (2)$$

$$\Delta S_m(T) = nR\ln(2S+1). \quad (3)$$

Conclusion

In conclusion, three clusters **1**-{Gd_2}, **2**-{Gd_6}, and **3**-{Gd_8} based on Schiff ligand H_2L were synthesized. Complex **1** contains two Gd^{III} ions, and magnetic measurement indicates antiferromagnetic interactions between the metal core, which is also confirmed by PHI fitting. Complexes **2** and **3** are hexa-nuclearity with a biaugmented trigonal prism configuration and octa-nuclearity with a cubic trapezoid structure. Magnetic investigations indicate the antiferromagnetic interactions between Gd^{III} ions are observed in complexes **2** and **3**. Magnetocaloric studies for complexes **1–3** show that the magnetic entropies of complexes **1–3** are smaller than the theoretical values, which is mainly caused by antiferromagnetic coupling. Furthermore, complex **1** exhibits a large magnetic

entropy of 25.05 J kg^{-1} K^{-1} at 2.0 K in di-nuclearity magnetic refrigerant materials, while complexes **2** and **3** belong to the normal range in hexa-nuclearity and octa-nuclearity complexes, respectively, demonstrating that they are promising molecular magnetic coolants for low-temperature cooling applications.

Data availability statement

The datasets presented in this study can be found in online repositories. The names of the repository/repositories and accession number(s) can be found in the article/Supplementary Material.

Author contributions

MW and CS: writing—original draft; YG, HX, LH, and YZ: investigation and formal analysis; JW: project administration and funding acquisition; YP: measurement; YT: validation, editing, and funding acquisition.

Funding

This work was supported by the National Natural Science Foundation of China (Nos. 22075152 and 22101144), the Natural Science Foundation of Jiangsu Province (No. BK20210835), and the Science and Technology Project Fund of Nantong (Nos. JC2020130, JC2020133, and JC2020134).

Acknowledgments

We are very grateful to the Nantong University Analytical Testing Center for its support for testing.

Conflict of interest

The authors declare that the research was conducted in the absence of any commercial or financial relationships that could be construed as a potential conflict of interest.

Publisher's note

Supplementary material

The Supplementary Material for this article can be found online at: https://www.frontiersin.org/articles/10.3389/fchem.2022.963203/full#supplementary-material

References

Adhikary, A., Sheikh, J. A., Biswas, S., and Konar, S. (2014). Synthesis, crystal structure and study of magnetocaloric effect and single molecular magnetic behaviour in discrete lanthanide complexes. *Dalton Trans.* 43, 9334–9343. doi:10.1039/C4DT00540F

Alvarez, S., Alemany, P., Casanova, D., Cirera, J., Llunell, M., and Avnir, D. (2005). Shape maps and polyhedral interconversion paths in transition metal chemistry. *Coord. Chem. Rev.* 249, 1693–1708. doi:10.1016/j.ccr.2005.03.031

Aronica, C., Pilet, G., Chastanet, G., Wernsdorfer, W., Jacquot, J.-F., and Luneau, D. (2006). A nonanuclear dysprosium(III)–copper(II) complex exhibiting single-molecule magnet behavior with very slow zero-field relaxation. *Angew. Chem. Int. Ed.* 45, 4659–4662. doi:10.1002/anie.200600513

Botezat, O., van Leusen, J., Kravtsov, V. C., Kogerler, P., and Baca, S. G. (2017). Ultralarge 3d/4f coordination wheels: From carboxylate/amino alcohol-supported $\{Fe_4Ln_2\}$ to $\{Fe_{18}Ln_6\}$ rings. *Inorg. Chem.* 56, 1814–1822. doi:10.1021/acs.inorgchem.6b02100

Boulon, M. E., Cucinotta, G., Luzon, J., Degl'Innocenti, C., Perfetti, M., Bernot, K., et al. (2013). Magnetic anisotropy and spin-parity effect along the series of lanthanide complexes with DOTA. *Angew. Chem. Int. Ed.* 52, 350–354. doi:10.1002/anie.201205938

Burgess, J. A., Malavolti, L., Lanzilotto, V., Mannini, M., Yan, S., Ninova, S., et al. (2015). Magnetic fingerprint of individual Fe_4 molecular magnets under compression by a scanning tunnelling microscope. *Nat. Commun.* 6, 8216–8222. doi:10.1038/ncomms9216

Casanova, D., Llunell, M., Alemany, P., and Alvarez, S. (2005). The rich stereochemistry of eight-vertex polyhedra: A continuous shape measures study. *Chem. Eur. J.* 11, 1479–1494. doi:10.1002/chem.200400799

Chandrasekhar, V., Das, S., Dey, A., Hossain, S., and Sutter, J.-P. (2013). Tetranuclear lanthanide (III) complexes containing dimeric subunits: Single-molecule magnet behavior for the Dy_4 analogue. *Inorg. Chem.* 52, 11956–11965. doi:10.1021/ic401652f

Chen, Q., Ma, F., Meng, Y.-S., Sun, H.-L., Zhang, Y.-Q., and Gao, S. (2016). Assembling dysprosium dimer units into a novel chain featuring slow magnetic relaxation via formate linker. *Inorg. Chem.* 55, 12904–12911. doi:10.1021/acs.inorgchem.6b02276

Chen, X.-M., Aubin, S. M. J., Wu, Y.-L., Yang, Y.-S., Mak, T. C. W., and Hendrickson, D. N. (1995). Polynuclear $Cu^{II}_{12}M^{III}_{6}$ (M = Y, Nd, or Gd) complexes encapsulating a ClO^{4-} anion: $[Cu_{12}M_6(OH)_{24}(H_2O)_{18}(pyb)_{12}(ClO_4)](ClO_4)_{17}\cdot nH_2O$ (pyb = pyridine betaine). *J. Am. Chem. Soc.* 117, 9600–9601. doi:10.1021/ja00142a043

Chen, Y.-C., Guo, F.-S., Zheng, Y.-Z., Liu, J.-L., Leng, J.-D., Tarasenko, R., et al. (2013). Gadolinium(III)-hydroxy ladders trapped in succinate frameworks with optimized magnetocaloric effect. *Chem. Eur. J.* 19, 13504–13510. doi:10.1002/chem.201301221

Chen, Y.-C., Qin, L., Meng, Z.-S., Yang, D.-F., Wu, C., Fu, Z., et al. (2014). Study of a magnetic-cooling material $Gd(OH)CO_3$. *J. Mat. Chem. A* 2, 9851–9858. doi:10.1039/C4TA01646G

Cornia, A., Rigamonti, L., Boccedi, S., Clerac, R., Rouzieres, M., and Sorace, L. (2014). Magnetic blocking in extended metal atom chains: A pentachromium(II) complex behaving as a single-molecule magnet. *Chem. Commun.* 50, 15191–15194. doi:10.1039/c4cc06693f

Dermitzaki, D., Raptopoulou, C. P., Psycharis, V., Escuer, A., Perlepes, S. P., and Stamatatos, T. C. (2015). Nonemployed simple carboxylate ions in well-investigated areas of heterometallic carboxylate cluster chemistry: A new family of $\{Cu^{II}_{4}Ln^{III}_{8}\}$

complexes bearing tert-butylacetate bridging ligands. *Inorg. Chem.* 54, 7555–7561. doi:10.1021/acs.inorgchem.5b01179

Dolomanov, O. V., Bourhis, L. J., Gildea, R. J., Howard, J. A. K., and Puschmann, H. (2009). OLEX2: A complete structure solution, refinement and analysis program. *J. Appl. Crystallogr.* 42, 339–341. doi:10.1107/S0021889808042726

Evangelisti, M., Roubeau, O., Palacios, E., Camón, A., Hooper, T. N., Brechin, E. K., et al. (2011). Cryogenic magnetocaloric effect in a ferromagnetic molecular dimer. *Angew. Chem. Int. Ed.* 50, 6606–6609. doi:10.1002/anie.201102640

Feltham, H. L. C., Dhers, S., Rouzières, M., Clérac, R., Powell, A. K., and Brooker, S. (2015). A family of fourteen soluble stable macrocyclic [NiIILnIII] heterometallic 3d–4f complexes. *Inorg. Chem. Front.* 2, 982–990. doi:10.1039/c5qi00130g

Feltham, H. L. C., Dumas, C., Mannini, M., Otero, E., Sainctavit, P., Sessoli, R., et al. (2017). Proof of principle: Immobilisation of robust CuII 3 TbIII-macrocycles on small, suitably pre-functionalised gold nanoparticles. *Chem. Eur. J.* 23, 2517–2521. doi:10.1002/chem.201604821

Guo, F.-S., Leng, J.-D., Liu, J.-L., Meng, Z.-S., and Tong, M.-L. (2012). Polynuclear and polymeric gadolinium acetate derivatives with large magnetocaloric effect. *Inorg. Chem.* 51, 405–413. doi:10.1021/ic2018314

Han, L.-J., Wang, W.-M., Wang, X.-W., Huai, L., Qiao, N., and Fang, M. (2021). A rhombic shaped {GdIII2CoII2} heterometallic cluster exhibiting larger cryogenic magnetocaloric effect. *Inorganica Chim. Acta* 514, 120020–120024. doi:10.1016/j.ica.2020.120020

Hou, Y.-L., Han, X., Hu, X.-Y., Shen, J.-X., Wang, J., Shi, Y., et al. (2020). Two LnIII4(LnIII = Gd and Dy) clusters constructed by 8-hydroxyquinoline schiff base and β-diketonate coligand: Magnetic refrigeration property and single-molecule magnet behavior. *Inorganica Chim. Acta* 502, 119290–119303. doi:10.1016/j.ica.2019.119290

Jiang, Y., Brunet, G., Holmberg, R. J., Habib, F., Korobkov, I., and Murugesu, M. (2016). Terminal solvent effects on the anisotropy barriers of Dy_2 systems. *Dalton Trans.* 45, 16709–16715. doi:10.1039/C6DT03366K

Kahn, M. L., Sutter, J.-P., Golhen, S., Guionneau, P., Ouahab, L., Kahn, O., et al. (2000). Systematic investigation of the nature of the coupling between a ln(III) ion (ln = Ce(III) to Dy(III)) and its aminoxyl radical ligands. Structural and magnetic characteristics of a series of {Ln(organic radical)$_2$} compounds and the related {Ln(Nitrone)$_2$} derivatives. *J. Am. Chem. Soc.* 122, 3413–3421. doi:10.1021/ja994175o

Lakma, A., Hossain, S. M., van Leusen, J., Kögerler, P., and Singh, A. K. (2019). Tetranuclear Mn^{II}, Co^{II}, Cu^{II} and Zn^{II} grid complexes of an unsymmetrical ditopic ligand: Synthesis, structure, redox and magnetic properties. *Dalton Trans.* 48, 7766–7777. doi:10.1039/C9DT01041F

Li, J. N., Li, N. F., Wang, J. L., Liu, X. M., Ping, Q. D., Zang, T. T., et al. (2021). A new family of boat-shaped Ln_8 clusters exhibiting the magnetocaloric effect and slow magnetic relaxation. *Dalton Trans.* 50, 13925–13931. doi:10.1039/d1dt02390j

Li, L.-F., Kuang, W.-W., Li, Y.-M., Zhu, L.-L., Xu, Y., and Yang, P.-P. (2019). A series of new octanuclear Ln_8 clusters: Magnetic studies reveal a significant cryogenic magnetocaloric effect and slow magnetic relaxation. *New J. Chem.* 43, 1617–1625. doi:10.1039/C8NJ04231D

Li, L., Yang, L.-R., Qiao, N., Xue, M.-M., Fang, Z.-X., Ren, J., et al. (2020). A novel tetranuclear Gd(III)-based cluster showing larger magnetic refrigeration property. *J. Mol. Struct.* 1222, 128906–128911. doi:10.1016/j.molstruc.2020.128906

Lin, Q.-F., Ding, L.-L., Xu, Z.-H., Wang, Q.-q., Li, N.-F., Xu, Y., et al. (2021). Three 3D Lanthanide coordination polymers: Synthesis, luminescence and magnetic properties. *J. Mol. Struct.* 1234, 130167–130173. doi:10.1016/j.molstruc.2021.130167

Liu, C.-M., and Hao, X. (2022). Asymmetric assembly of chiral lanthanide(III) tetranuclear cluster complexes using achiral mixed ligands: Single-molecule magnet behavior and magnetic entropy change. *ACS Omega* 7, 20229–20236. doi:10.1021/acsomega.2c02155

Liu, J.-L., Chen, Y.-C., Guo, F.-S., and Tong, M.-L. (2014). Recent advances in the design of magnetic molecules for use as cryogenic magnetic coolants. *Coord. Chem. Rev.* 281, 26–49. doi:10.1016/j.ccr.2014.08.013

Liu, J.-L., Chen, Y.-C., and Tong, M.-L. (2016). Molecular design for cryogenic magnetic coolants. *Chem. Rec.* 16, 825–834. doi:10.1002/tcr.201500278

Lu, G., Wang, J., Zhang, C.-J., Bala, S., Chen, Y.-C., Huang, G.-Z., et al. (2019). Single-ion magnet and luminescent properties in a Dy(III) triangular dodecahedral complex. *Inorg. Chem. Commun.* 102, 16–19. doi:10.1016/j.inoche.2019.02.003

Luan, F., Liu, T., Yan, P., Zou, X., Li, Y., and Li, G. (2015). Single-molecule magnet of a tetranuclear dysprosium complex disturbed by a salen-type ligand and chloride counterions. *Inorg. Chem.* 54, 3485–3490. doi:10.1021/acs.inorgchem.5b00061

Mannini, M., Bertani, F., Tudisco, C., Malavolti, L., Poggini, L., Misztal, K., et al. (2014). Magnetic behaviour of $TbPc_2$ single-molecule magnets chemically grafted on silicon surface. *Nat. Commun.* 5, 4582–4589. doi:10.1038/ncomms5582

Mayans, J., and Escuer, A. (2021). Correlating the axial zero field splitting with the slow magnetic relaxation in Gd^{III} SIMs. *Chem. Commun.* 57, 721–724. doi:10.1039/D0CC07474H

Milios, C. J., Inglis, R., Vinslava, A., Bagai, R., Wernsdorfer, W., Parsons, S., et al. (2007). Toward a magnetostructural correlation for a family of Mn_6 SMMs. *J. Am. Chem. Soc.* 129, 12505–12511. doi:10.1021/ja0736616

Nava, A., Rigamonti, L., Zangrando, E., Sessoli, R., Wernsdorfer, W., and Cornia, A. (2015). Redox-controlled exchange bias in a supramolecular chain of Fe_4 single-molecule magnets. *Angew. Chem. Int. Ed.* 54, 8777–8782. doi:10.1002/anie.201500897

Neves, A., Erthal, S. M. D., Vencato, I., Ceccato, A. S., Mascarenhas, Y. P., Nascimento, O. R., et al. (1992). Synthesis, crystal structure, electrochemical, and spectroelectrochemical properties of the new manganese(III) complex [Mn^{III}(BBPEN)] [PF_6] [H_2BBPEN = N, N'-bis(2-hydroxybenzyl)-N, N'-bis(2-methylpyridyl)ethylenediamine]. *Inorg. Chem.* 31, 4749–4755. doi:10.1021/ic00049a008

Oyarzabal, I., Ruiz, J., Seco, J. M., Evangelisti, M., Camon, A., Ruiz, E., et al. (2014). Rational electrostatic design of easy-axis magnetic anisotropy in a Zn(II)-Dy(III)-Zn(II) single-molecule magnet with a high energy barrier. *Chem. Eur. J.* 20, 14262–14269. doi:10.1002/chem.201403670

Pecharsky, V. K., and Gschneidner, J. K. A. (1997). Giant magnetocaloric effect in $Gd_5\{Si_2Ge_2$. *Phys. Rev. Lett.* 78, 4494–4497. doi:10.1103/PhysRevLett.78.4494

Pecharsky, V. K., and Gschneidner, K. A. Jr (1999). Magnetocaloric effect and magnetic refrigeration. *J. Magn. Magn. Mat.* 200, 44–56. doi:10.1016/S0304-8853(99)00397-2

Reis, M. S. (2020). Magnetocaloric and barocaloric effects of metal complexes for solid state cooling: Review, trends and perspectives. *Coord. Chem. Rev.* 417, 213357. doi:10.1016/j.ccr.2020.213357

Ren, J., Wei, X. Q., Xu, R. S., Chen, Z. Y., Wang, J., Wang, M., et al. (2021). A potential ferromagnetic lanthanide–transition heterometallic molecular–based bacteriostatic agent. *J. Mol. Struct.* 1229, 129783. doi:10.1016/j.molstruc.2020.129783

Shang, Y., Cao, Y., Xie, Y., Zhang, S., and Cheng, P. (2021). A 1D Mn-based coordination polymer with significant magnetocaloric effect. *Polyhedron* 202, 115173–115179. doi:10.1016/j.poly.2021.115173

Sheldrick, G. M. (2015a). Crystal structure refinement with SHELXL. *Acta Crystallogr. C Struct. Chem.* C71, 3–8. doi:10.1107/S2053229614024218

Sheldrick, G. M. (2015b). Shelxt - integrated space-group and crystal-structure determination. *Acta Crystallogr. A Found. Adv.* A71, 3–8. doi:10.1107/S2053273314026370

Shen, H.-Y., Wang, W.-M., Bi, Y.-X., Gao, H.-L., Liu, S., and Cui, J.-Z. (2015). Luminescence, magnetocaloric effect and single-molecule magnet behavior in lanthanide complexes based on a tridentate ligand derived from 8-hydroxyquinoline. *Dalton Trans.* 44, 18893–18901. doi:10.1039/c5dt02894a

Shi, Q.-H., Xue, C.-L., Fan, C.-J., Yan, L.-L., Qiao, N., Fang, M., et al. (2021). Magnetic refrigeration property and slow magnetic relaxation behavior of five dinuclear Ln(III)-based compounds. *Polyhedron* 194, 114938. doi:10.1016/j.poly.2020.114938

Shi, X.-H., Hao, S.-S., Wang, M.-J., Zhang, L., Liang, W.-H., Gao, H.-M., et al. (2020). Two $Ln(III)_2$ (Ln = Gd and Dy) compounds showing magnetic refrigeration and slow magnetic relaxation. *J. Mol. Struct.* 1210, 127997. doi:10.1016/j.molstruc.2020.127997

Wang, J., Wu, Z.-L., Yang, L.-R., Xue, M.-M., Fang, Z.-X., Luo, S.-C., et al. (2021a). Two lanthanide-based dinuclear clusters (Gd_2 and Dy_2) with schiff base derivatives: Synthesis, structures and magnetic properties. *Inorganica Chim. Acta* 514, 120015. doi:10.1016/j.ica.2020.120015

Wang, M., Lu, L., Song, W., Wang, X., Sun, T., Zhu, J., et al. (2021b). AIE-active Schiff base compounds as fluorescent probe for the highly sensitive and selective detection of Al^{3+} ions. *J. Lumin.* 233, 117911. doi:10.1016/j.jlumin.2021.117911

Wang, W.-M., Gao, Y., Yue, R.-X., Qiao, N., Wang, D.-T., Shi, Y., et al. (2020c). Construction of a family of Ln_3 clusters using multidentate schiff base and β-diketonate ligands: Fluorescence properties, magnetocaloric effect and slow magnetic relaxation. *New J. Chem.* 44, 9230–9237. doi:10.1039/d0nj01172j

Wang, W.-M., He, L.-Y., Wang, X.-X., Shi, Y., Wu, Z.-L., and Cui, J.-Z. (2019b). Linear-shaped LnIII 4 and LnIII 6 clusters constructed by a polydentate schiff base ligand and a *β*-diketone co-ligand: Structures, fluorescence properties, magnetic refrigeration and single-molecule magnet behavior. *Dalton Trans.* 48, 16744–16755. doi:10.1039/c9dt03478a

Wang, W.-M., Huai, L., Wang, X.-W., Jiang, K.-J., Shen, H.-Y., Gao, H.-L., et al. (2020d). Structures, magnetic refrigeration and single molecule-magnet behavior of five rhombus-shaped tetranuclear Ln(III)-based clusters. *New J. Chem.* 44, 10266–10274. doi:10.1039/d0nj01969k

Wang, W.-M., Wang, M.-J., Hao, S.-S., Shen, Q.-Y., Wang, M.-L., Liu, Q.-L., et al. (2020a). 'Windmill'-shaped LnIII 4 (LnIII = Gd and Dy) clusters: Magnetocaloric effect and single-molecule-magnet behavior. *New J. Chem.* 44, 4631–4638. doi:10.1039/c9nj05317d

Wang, W.-M., Xue, C.-L., Jing, R.-Y., Ma, X., Yang, L.-N., Luo, S.-C., et al. (2020b). Two hexanuclear lanthanide Ln_6^{III} clusters featuring remarkable magnetocaloric effect and slow magnetic relaxation behavior. *New J. Chem.* 44, 18025–18030. doi:10.1039/D0NJ03442H

Wang, W.-M., Yue, R.-X., Gao, Y., Wang, M.-J., Hao, S.-S., Shi, Y., et al. (2019a). Large magnetocaloric effect and remarkable single-molecule-magnet behavior in triangle-assembled LnIII 6 clusters. *New J. Chem.* 43, 16639–16646. doi:10.1039/C9NJ03921J

Wang, W.-M., Zhang, H.-X., Wang, S.-Y., Shen, H.-Y., Gao, H.-L., Cui, J.-Z., et al. (2015). Ligand field affected single-molecule magnet behavior of lanthanide(III) dinuclear complexes with an 8-hydroxyquinoline Schiff base derivative as bridging ligand. *Inorg. Chem.* 54, 10610–10622. doi:10.1021/acs.inorgchem.5b01404

Wang, Y. -X., Xu, Q., Ren, P., Shi, W., and Cheng, P. (2019c). Solvent-induced formation of two gadolinium clusters demonstrating strong magnetocaloric effects and ferroelectric properties. *Dalton Trans.* 48, 2228–2233. doi:10.1039/c8dt04267e

Wei, W., Wang, X., Zhang, K., Tian, C.-B., and Du, S.-W. (2019). Tuning the topology from fcu to pcu: Synthesis and magnetocaloric effect of metal–organic frameworks based on a hexanuclear Gd(III)-hydroxy cluster. *Cryst. Growth Des.* 19, 55–59. doi:10.1021/acs.cgd.8b01566

Wei, W., Xie, R.-K., Du, S.-W., Tian, C.-B., and Chai, G.-L. (2021). Synthesis, structure, magnetocaloric effect and DFT calculations of a Mn^{II} cluster-based inorganic coordination polymer. *J. Alloys Compd.* 878, 160353–160361. doi:10.1016/j.jallcom.2021.160353

Wu, D. Q., Zhang, M. L., Li, Z. Y., Zhang, P. P., Zhang, M. Y., Wu, C. F., et al. (2021). A two dimensional Gd^{III} coordination polymer based on isonicotinic acid N-oxide with large magnetocaloric effect. *Z. Anorg. Allg. Chem.* 647, 1542–1546. doi:10.1002/zaac.202100033

Wu, T. X., Tao, Y., He, Q. J., Li, H. Y., Bian, H. D., and Huang, F. P. (2021). Constructing an unprecedented {MnII 38} matryoshka doll with a [Mn 18(CO3) 9] inorganic core and magnetocaloric effect. *Chem. Commun.* 57, 2732–2735. doi:10.1039/d0cc07884k

Xu, C., Wu, Z., Fan, C., Yan, L., Wang, W., and Ji, B. (2021). Synthesis of two lanthanide clusters LnIII 4 (Gd 4 and Dy 4) with [2×2] square grid shape: Magnetocaloric effect and slow magnetic relaxation behaviors. *J. Rare Earths* 39, 1082–1088. doi:10.1016/j.jre.2020.08.015

Yao, X., Yan, P., An, G., Li, Y., Li, W., and Li, G. (2018). Investigation of magneto-structural correlation based on a series of seven-coordinated beta-diketone Dy(iii) single-ion magnets with C_{2v} and C_{3v} local symmetry. *Dalton Trans.* 47, 3976–3984. doi:10.1039/c7dt04764a

Yin, D.-D., Chen, Q., Meng, Y.-S., Sun, H.-L., Zhang, Y.-Q., and Gao, S. (2015). Slow magnetic relaxation in a novel carboxylate/oxalate/hydroxyl bridged dysprosium layer. *Chem. Sci.* 6, 3095–3101. doi:10.1039/c5sc00491h

Zhang, L., Jung, J., Zhang, P., Guo, M., Zhao, L., Tang, J., et al. (2016). Site-resolved two-step relaxation process in an asymmetric Dy_2 single-molecule magnet. *Chem. Eur. J.* 22, 1392–1398. doi:10.1002/chem.201503422

Zhang, L., Zhang, Y.-Q., Zhang, P., Zhao, L., Guo, M., and Tang, J. (2017). Single-molecule magnet behavior enhanced by synergic effect of single-ion anisotropy and magnetic interactions. *Inorg. Chem.* 56, 7882–7889. doi:10.1021/acs.inorgchem.7b00625

Zhang, P., Zhang, L., Lin, S.-Y., and Tang, J. (2013). Tetranuclear $[MDy]_2$ compounds and their dinuclear [MDy] (M = Zn/Cu) building units: Their assembly, structures, and magnetic properties. *Inorg. Chem.* 52, 6595–6602. doi:10.1021/ic400620j

Zhang, S., -W., Duan, E., and Cheng, P. (2015b). An exceptionally stable 3D GdIII-organic framework for use as a magnetocaloric refrigerant. *J. Mat. Chem. A Mat.* 3, 7157–7162. doi:10.1039/c4ta06209d

Zhang, S., and Cheng, P. (2016). Coordination-cluster-based molecular magnetic refrigerants. *Chem. Rec.* 16, 2077–2126. doi:10.1002/tcr.201600038

Zhang, S., Duan, E., Han, Z., Li, L., and Cheng, P., (2015a). Lanthanide coordination polymers with 4, 4'-azobenzoic acid: Enhanced stability and magnetocaloric effect by removing guest solvents. *Inorg. Chem.* 54, 6498–6503. doi:10.1021/acs.inorgchem.5b00797

Zhao, X. Q., Wang, J., Bao, D. X., Xiang, S., Liu, Y. J., and Li, Y. C. (2017). The ferromagnetic $[Ln_2Co_6]$ heterometallic complexes. *Dalton Trans.* 46, 2196–2203. doi:10.1039/c6dt04375e

Zheng, T.-F., Tian, X.-M., Ji, J., Luo, H., Yao, S.-L., Liu, S.-J., et al. (2020). Two Gd_2 cluster complexes with monocarboxylate ligands displaying significant magnetic entropy changes. *J. Mol. Struct.* 1200, 127094. doi:10.1016/j.molstruc.2019.127094

Zhou, M., Wu, L.-H., Wu, X.-Y., Yao, S.-L., Zheng, T.-F., Xie, X., et al. (2021). Two dinuclear Gd^{III} clusters based on isobutyric acid and nicotinic acid with large magnetocaloric effects. *J. Mol. Struct.* 1227, 129689. doi:10.1016/j.molstruc.2020.129689

Zhu, J., Wang, C., Luan, F., Liu, T., Yan, P., and Li, G. (2014). Local coordination geometry perturbed beta-diketone dysprosium single-ion magnets. *Inorg. Chem.* 53, 8895–8901. doi:10.1021/ic500501r